arXiv:cond-mat/9805053v1 [cond-mat.mes-hall] 5 May 1998

# Single-electron-parametron-based logic devices

Alexander N. Korotkov[1,2] and Konstantin K. Likharev[1]

[1]*Department of Physics, State University of New York, Stony Brook, NY 11794-3800 and* [2]*Nuclear Physics Institute, Moscow State University, Moscow 119899, Russia.*

(December 5, 2017)

## Abstract

We analyze the operation of the wireless single-electron logic family based on single-electron-parametron cells. Parameter margins, energy dissipation, and the error probability are calculated using the orthodox theory of single-electron tunneling. Circuits of this family enable quasi-reversible computation with energy dissipation per bit much lower than the thermal energy, and hence may circumvent one of the main obstacles faced by ultradense three-dimensional integrated digital circuits.

Typeset using REVTEX

## I. INTRODUCTION

Single-electron tunneling[1,2] in systems of small-capacitance tunnel junctions has attracted much attention during the last decade because of both the interesting physics and the possibility of useful devices. Today the basic physics of single-electron tunneling is sufficiently well understood, and its possible applications (for reviews see, e.g., Refs.[3] and[4]) are becoming an important issue. The practical value of several analog applications has already been proven: for example, the single-electron transistor[5,6] as a highly sensitive electrometer,[7] the single-electron pump[8] as a standard of dc current,[9] and the array of tunnel junctions[10] as an absolute thermometer.[11]

In the field of digital electronics, however, only rudimentary devices have been demonstrated so far.[12–18] The recent invention[19] of hybrid circuits based on single-electron-transistor readout from floating-gate memory cells presumably opens a way to room-temperature *memories* with density beyond $10^{11}$ bit/cm$^2$. (This concept has been supported by recent experiments[18] with the first low-temperature prototypes of such memory cells). The potential of single-electronics in *logic* circuits, however, remains uncertain due to substantial problems which have to be solved for both types of single-electron logic devices suggested so far.

Devices of the first type use single-electron transistors instead of field effect transistors in "voltage-state" circuits similar to conventional digital electronics.[7] In these devices the effects of charge quantization are restricted to the interior of the single-electron transistors. As a result, the design of such circuits (including complementary[20]) is relatively straightforward. They suffer, however, from a relatively high static power consumption.[21,22]

The second possible way (which allows to reduce the power dissipation), is to code bits directly by single electrons everywhere in the circuit.[23–32] (A different, interesting approach based on rf parametric excitation of single-electron-tunneling oscillations has been suggested by Kiel and Oshima;[33] unfortunately their original proposal seems to have run into considerable implementation problems[34]). It is important that these "charge-state" logic circuits

do not necessarily require long wires and can be implemented using only small conducting islands separated by tunnel barriers, with the necessary power and timing provided by an external rf electric field.[27] Recently we suggested[28] a new device for charge-state, wireless logic circuits - the Single Electron Tunneling Parametron (or SET Parametron). In comparison with the wireless single-electron devices suggested earlier,[27] the SET Parametron may have wider parameter margins and extremely low power dissipation, lower than the thermodynamic "limit" of $k_B T \ln 2$ per bit.[29]

In this paper we present the results of a detailed analysis of the SET Parametron and basic logic circuits using this device. The major characteristics of the SET Parametron, including its parameter margins, speed, error rate, and power consumption, will be discussed.

## II. SET PARAMETRON: THE BASIC IDEA

The basic cell of the new logic family, the SET Parametron, consists of three conducting islands - see Fig. 1a. (In our numerical calculations we have assumed the islands to be of spherical shape, with $R$ being the radius of the edge islands 1 and 3, and $r$ the radius of the middle island 2; this assumption is, however, not important for the device operation.) The middle island is slightly shifted off the line passing through the centers of the edge islands. We will identify this line with $x$-axis, and the direction of the middle island shift with $y$-axis (which is the symmetry axis of the cell). Electrons can tunnel through small gaps between the middle and edge islands, but not directly between the edge islands because of their much larger spacing (Fig. 1a).

Let us assume that the cell as a whole is charged by one uncompensated electron. (This assumption makes the explanation of the operation principle simpler; later we will consider the more natural case of an initially neutral cell.) If the cell is biased with a sufficiently strong "clock" electric field $E_c > 0$ directed along axis $y$, the electron is obviously located at the central island.[35] Now let the field be decreased gradually so that eventually it changes direction to negative. At some moment the electron will have to tunnel to one of the edge

islands because these states become energetically preferable. Because of the geometrical symmetry, the choice of island (left or right) will be random, i.e. the charge symmetry of the system will be broken spontaneously.

However, if there is a weak "signal" field $E_s$ along direction $x$ (this field may be applied, for example, by the neighboring similar cell), the final position of the electron will depend on the sign of $E_s$. A natural way to discuss this effect is to say that the signal field $E_s$ creates an energy difference $\Delta$ between the electron states in islands 1 and 3, and that the electron prefers to tunnel into the island with the lowest energy state (Fig. 1b). If now the clock field $E_c$ becomes negative and large, it creates a high energy barrier $W$ (see Fig. 1b) between the edge islands, so that the electron is reliably trapped in the island it has tunneled to, regardless of further changes of the signal field $E_s$.

Thus if fluctuations in the system are low enough, and the clock field changes slowly enough, even a small field $E_s$ of the proper sign at the decision-making moment (when $W(t)=0$) is sufficient to ensure a certain robust final polarization of the cell. This process can be interpreted as a reliable recording of one bit of information; for example, the electron on the right island may mean logical "1" while the electron on the left island encode logical "0". Now the dipole moment of the cell can in turn be used to produce the signal field to control the other cells during their decision-making moments, and hence determine their information contents (see Section V below).

This "parametric" amplification of signal, which gave the SET Parametron its name, is quite similar to the operation of a Josephson junction device called Parametric Quantron[36,37] (re-invented later as the "Flux Quantum Parametron"[38]), and in a broader sense to rf-driven parametrons.[39,33] The main difference is that all the previously analyzed parametrons are described by a continuous degree of freedom (e.g., the Josephson phase $\phi$ in the Parametric Quantron). This variable can take any value, and the discrete information states correspond to energy minima on the $\phi$ axis. On the other hand, in the SET Parametron with low tunnel conductances, the possible states are discrete (the electron has to be definitely on one of the islands at each particular instant).[40]

## III. SET PARAMETRON: QUANTITATIVE ANALYSIS

Let us consider the operation of one SET Parametron cell using the orthodox theory[1] which is adequate for the description of single-electron tunneling in systems with many background electrons in each island and sufficiently low conductance $G$ of tunnel junctions ($G \ll e^2/\hbar$). In this theory the electron is always localized in one of the islands, and the rate $\Gamma$ of each tunneling event is solely determined by the corresponding decrease $W = -\Delta\varepsilon$ of electrostatic energy $\varepsilon$ of the system. Using elementary electrostatics, we obtain the following expressions for the energy decreases corresponding to four possible tunneling events in the SET Parametron (tunneling to/from each of the edge islands is denoted with signs + and −, respectively):

$$\begin{aligned} W_l^{\pm} &= \pm e\,(\phi_2 - \phi_1) - W_{12}, \\ W_r^{\pm} &= \pm e\,(\phi_2 - \phi_3) - W_{23}\,, \end{aligned} \tag{1}$$

$$\phi_i = \sum_{j=1}^{3} (C^{-1})_{ij} q_j - \vec{E}\vec{D}_i\,, \tag{2}$$

$$W_{ij} = \frac{e^2}{2}\left[(C^{-1})_{ii} + (C^{-1})_{jj} - 2(C^{-1})_{ij}\right]\,, \tag{3}$$

$$q_i = q_{i0} + n_i e\,. \tag{4}$$

Here $l(r)$ means left (right) junction, $\phi_i$ is the electrostatic potential of $i$-th island (for numbering, see Fig. 1a), $W_{12}$ and $W_{23}$ are the Coulomb blockade energies, and $C^{-1}$ is the inverse capacitance matrix. Vectors $e\vec{D}_i = (eD_{ix}, eD_{iy}, eD_{iz})$ are the dipole moments of islands when charged with single electrons, $\vec{E}$ is the external electric field (accepted to be uniform) and $q_i$ is the total electric charge of $i$-th island, while $q_{i0}$ is the uncompensated part of its background charge.

In the limit when the island radii are smaller than the spacing between islands, the following simple approximation for the capacitance matrix elements can be used:

$$
\begin{aligned}
&(C^{-1})_{11} = (C^{-1})_{33} = \frac{1}{4\pi\epsilon\epsilon_0}\,\frac{1}{R}\,; \quad (C^{-1})_{22} = \frac{1}{4\pi\epsilon\epsilon_0}\,\frac{1}{r}\,; \\
&(C^{-1})_{ij} = \frac{1}{4\pi\epsilon\epsilon_0}\,\frac{1}{s_{ij}}\,, \quad i \neq j\,; \\
&s_{ij} = \left[(x_i - x_j)^2 + (y_i - y_j)^2 + (z_i - z_j)^2\right]^{1/2}; \\
&\vec{D}_i = \vec{r}_i, \qquad (5)
\end{aligned}
$$

where $\vec{r}_i = (x_i, y_i, z_i)$ is the $i$-th island center, and $\epsilon$ is the dielectric constant of the dielectric environment. In the case of comparable radii and island spacing, $C_{ij}$ have to be calculated numerically, for example, using the method of multiple electrostatic images (see Appendix A). The results show that approximation (5) gives accuracy better than 10% if the spacing between the islands is larger than the largest island's radius.

In our initial analysis (until Section VII) we will assume that temperature $T$ is low and that the electric fields are changing slowly (adiabatically). In this case the full result of the orthodox theory,

$$
\Gamma = \frac{G\,W}{e^2\,[1 - \exp(-W/k_B T)]} \qquad (6)
$$

is reduced to the simple rule that the system always follows the local minimum of the total electrostatic energy.

Figure 2a shows the phase diagram of stationary charge states of a cell charged by one uncompensated electron. Each state is locally stable within a diamond-shape region corresponding to two conditions:

$$
|e(\phi_2 - \phi_1)| < W_{12}\,, \quad |e(\phi_2 - \phi_3)| < W_{23}\,, \qquad (7)
$$

being valid simultaneously, so that no tunneling event is possible, $W^{\pm}_{l,r} < 0$. Within the small-island approximation (5) the position of the diamond center is

$$
\begin{aligned}
E_s &= \frac{1}{4\pi\epsilon\epsilon_0}\,\frac{1}{2}\,\frac{1}{d}\,(n_1 - n_3)\,e\left(\frac{1}{2d} - \frac{1}{R}\right), \\
E_c &= \frac{1}{4\pi\epsilon\epsilon_0}\,\frac{1}{2}\,\frac{1}{b}\left[(n_1 + n_3)\,e\left(\frac{2}{s} - \frac{1}{2d} - \frac{1}{R}\right)\right. \\
&\quad \left. +2n_2 e\left(\frac{1}{r} - \frac{1}{s}\right)\right], \qquad (8)
\end{aligned}
$$

while the diamond width and height are

$$\delta E_s = \frac{2}{e}\frac{1}{d}W_{12}\,, \quad \delta E_c = \frac{2}{e}\frac{1}{b}W_{12}\,,$$
$$W_{12} = W_{23} = \frac{e^2}{2}\frac{1}{4\pi\epsilon\epsilon_0}\left(\frac{1}{r}+\frac{1}{R}-\frac{2}{s}\right) \tag{9}$$

(here $s \equiv s_{12} = s_{23} = (d^2+b^2)^{1/2}$ is the distance between island centers – see Fig. 1a).

The diamonds are periodic along both axes $E_s$ and $E_c$, with periods

$$\Delta E_s = \frac{1}{4\pi\epsilon\epsilon_0}\frac{1}{d}\,e\left(\frac{1}{R}-\frac{1}{2d}\right),$$
$$\Delta E_c = \frac{1}{4\pi\epsilon\epsilon_0}\frac{1}{b}\,e\left(\frac{1}{R}+\frac{2}{r}+\frac{1}{2d}-\frac{4}{s}\right). \tag{10}$$

Equations (8)–(10) are valid even if the approximation (5) is not used; however, in this case $1/R$, $1/r$, $1/s$, $1/2d$ (divided by $4\pi\epsilon\epsilon_0$) need to be replaced by $C_{11}^{-1}$, $C_{22}^{-1}$, $C_{12}^{-1}$, $C_{13}^{-1}$, respectively, and also $b$ and $d$ by $D_{2y}-D_{1y}$ and $D_{2x}-D_{1x}$ (the corresponding equations are direct consequences of Eqs. (1)–(3) and (7)).

The period along axis $E_s$ corresponds to the transformation $(n_1, n_2, n_3) \to (n_1-1, n_2, n_3+1)$, while the period along $E_c$ axis corresponds to $(n_1, n_2, n_3) \to (n_1-1, n_2+2, n_3-1)$. Notice that these transformations allow only even-number changes at the middle island; the "odd" set of diamonds can be obtained from the "even" set by the shift $(\Delta E_s/2, \Delta E_c/2)$.

Figure 2a shows the results of more exact, numerical calculations of the phase diagram for a particular cell; however, they are quite close to the approximate analytical results (8)–(10). (The approximation accuracy is better than 10% and it becomes even better than 1% after the normalization by $\Delta E_s$ and $\Delta E_c$.) For example, the minor offset of the diamond corners from the horizontal axis, which arises due to deviations from the analytical approximation, is hardly visible.

The most important qualitative feature of the phase diagram is the existence of bistability regions (shaded in Fig. 2a) where either of two charge states is locally stable. We will refer to the SET Parametron in these regions as being in an ON state, while the remaining part of the phase diagram corresponds to one of the possible OFF states of the system. If signal field $E_s$ is low (as we suppose in the following), only the set of diamonds along axis $E_c$

may be implemented. The arrow in Fig. 2a shows a possible way (described qualitatively in Sec. II above) of switching the cell from a monostable OFF state to a bistable ON state by changing the clock field $E_c$. It is clear that the sign of a small $E_s$ field determines which diamond boundary will be crossed first, and hence determines the charge state of the system within this bistable region.

Notice that crossing any phase boundary outside of the bistable regions involves one tunneling event with negligible energy difference $W$. In the adiabatic limit this transition is reversible, and the associated energy loss is infinitesimal (see Sec. VII). However, leaving the bistable state from the state with higher energy results in two sequential tunneling events and leads to a finite energy loss. This irreversible switching should be avoided in reversible computation. Below we will show that SET Parametron circuits can operate using exclusively reversible transitions.

## IV. SINGLE EXCITON PARAMETRON

While the case of the cell charged by one electron is the simplest for understanding the device operation, a more natural option is the initially electrically neutral cell: $n_1+n_2+n_3 = 0$. (This variety of SET Parametrons may be called the "Single Exciton Parametron", since digital bits in it are presented by electrostatically bound electron-hole pairs, although the physics of this bound state is rather different from that of the usual excitons in semiconductors.) Figure 2b shows the phase diagram of such a cell with the same geometrical parameters as in Fig. 2a. The only difference between the diagrams is a change in the charge states labeling and a fixed shift along $E_c$ axis, so that the diagram in Fig. 2b is symmetric about both axes. (Actually, *any* change of the initial charge of the cell is equivalent to a fixed offset of the fields $E_c$ and $E_s$).

Due to its field sign symmetry, the Single Exciton Parametron allows two natural modes of operation. The first is illustrated by the arrowed rectangle in the center of the diagram (instead of the thick line in Fig. 2a we have drawn the rectangle in Fig. 2b to emphasize that

$E_s$ may shift during the operation). The periodic clock field $E_c(t)$ causes two switchings OFF→ON and two switchings ON→OFF per period. Another possible mode of operation is shown by the smaller rectangle centered at $E_s$=$\Delta E_s/2$. It also provides two pairs of ON/OFF switchings per period of the clock field $E_c(t)$, with the bistable state implemented at small fields. In our analysis we will concentrate on the former operation mode because it does not require the additional dc bias of the signal field, though the latter mode may allow wider parameter margins.

Figures 2a and 2b show the phase diagrams of SET Parametrons for a particular set of geometric parameters. Changing the parameters may result not only in quantitative but also qualitative changes of the diagram. In particular, regions with three stable charge states appear if the ratio $\delta E_s/\Delta E_s$ of the diamond width and period becomes larger than 2; if the ratio is larger than 3, four states can coexist, and so on. Geometrically the multi-stability requires a smaller middle island to increase the Coulomb barrier for the electron transfer between the edge islands via the middle island. For the sake of simplicity we will limit ourselves to the bistable case.[41]

## V. SHIFT REGISTER

Figure 3 shows the standard scheme of operation of a shift register using parametron-type binary cells.[39] In this figure, each symbol represents a parametron cell at some particular phase of the periodic switching process. Dash means the monostable (OFF) state, while $\mathbf{I_i}$ means the $i$-th data bit which can be either "0" or "1". Evolution of the symbols shows the bit flow when the cells are periodically switched ON and OFF using periodic clock signals which are shifted by $2\pi/3$ for each next stage of the register.

In the initial state (upper line) each bit is encoded by the corresponding ON state of only one parametron. The signal field created by this cell is exerted on both neighboring cells, initially in their OFF state. Due to this field, when the right neighboring cell is switched from OFF to ON by the clock field (second line in Fig. 3), its logic state will be determined

by that of the initial cell. Now when the information has been copied to the right cell, the initial cell can be switched OFF (third line of Fig. 3). Thus, the information has been moved by one cell (one register stage), and the process may be repeated again (lines 4 to 7) and again. Notice that unidirectionality of the bit propagation is achieved by the "running wave" of the clock while the structure itself is 1D-isotropic.

During each period of the three-phase clock, the information is shifted by three stages, so that we need 3 cells per bit of information. It is straightforward to increase the number of phases beyond 3. Typically this would make the system more robust, but require proportionally more hardware per bit. (More generally, the number of cells per bit has not to be integer: by changing the clock phase shift it can have any value larger than 2).

Figure 4 shows a natural implementation of shift register using Single Exciton Parametron cells.[28] Each next cell, the direction of the middle island shift is turned by $\pi/3$ (within plane $y-z$). The system is driven by the clock field vector $\vec{E}(t)$ rotating in the same plane. This rotation provides the shift of $E_c$ (which is now the component of the clock field in the plane of the corresponding cell) by 1/6 of the clock period for each next cell. When a cell is in ON state, its dipole electric moment creates the signal field $E_s$ which is especially strong for its nearest neighbors, and thus determines the direction of electron tunneling when one of the neighbors in turned ON.

The operation of the system is illustrated in Fig. 5. Three sine lines show the in-plane components of the clock field for each of three neighboring cells. Since the operation cycle corresponds to the central rectangle shown in Fig. 2b, it differs slightly from the traditional mode shown in Fig. 3: each cell is switched OFF and ON twice per clock period.[42] In the simplest case of weak coupling when the signal field $E_s$ is much smaller than the clock field amplitude, switchings happen when the clock field $E_c$ crosses one of the thresholds $\pm\delta E_c/2$ and the cell enters or leaves the bistable region (shaded in Fig. 5). For correct operation of the shift register, switching OFF$\rightarrow$ON of a cell (see, e.g., point $S$ at the thicker middle curve) should occur when the previous neighboring cell is in ON state while the next neighboring cell is in OFF state, just as shown in Fig. 5.

In order to find the width of parameter window corresponding to correct operation of the parametron, let us first neglect the inter-cell interaction. Using the operation diagram shown in Fig. 5 and the phase diagram of Fig. 2b it is straightforward to obtain that the amplitude $A$ of the rotating clock field has to satisfy the following three conditions:

$$\begin{aligned} & A\sin(\frac{\pi}{2}-\frac{\theta}{2}) > \frac{\delta E_c}{2}\,, \\ & A\sin(\frac{\theta}{2}) < \frac{\delta E_c}{2}\,, \\ & A < \Delta E_c - \frac{\delta E_c}{2}\,. \end{aligned} \tag{11}$$

where $\theta$ is the clock phase shift between the adjacent cells. The first condition is necessary to have the signal source cell still in ON state when a recipient cell switches from OFF to ON. The second relation ensures that at that instant the next cell is already in OFF state. Finally, the third inequality means that the clock field does not reach the next diamond at the $E_c$ axis - see Fig. 2b and Eqs. (9) and (10), so that no undesirable charge states appear during the operation.

Equations (11) can be reduced to the following equation for the one-side margin $\xi$ of the field amplitude, $\xi \equiv (A_{max} - A_{min})/(A_{max} + A_{min})$:

$$\xi = \min\left[\tan(\frac{\pi}{4}-\frac{\theta}{2}),\ \frac{2\Delta E_c/\delta E_c - 1 - 1/\cos(\theta/e)}{2\Delta E_c/\delta E_c - 1 + 1/\cos(\theta/e)}\right]. \tag{12}$$

Within the approximation (5) the ratio $\Delta E_c/\delta E_c$ is equal to $2-(1/R-1/2d)/(1/R+1/r-2/s)$; this ratio increases when the radius of the middle island decreases. In the general case when the terms $1/R$, $1/r$, $1/2d$, and $1/s$ are replaced for the elements of the inverse capacitance matrix, the upper bound for $\Delta E_c/\delta E_c$ is equal to 2, while the lower bound is equal to 1.[41]

For the particular case shown in Fig. 4 we have $\theta = 2\pi/6$, hence, Eq. (12) gives the maximum margin of $\xi = \tan(\pi/12) \simeq 27\%$ for the amplitude $A$ of the rotating clock field if $\Delta E_c/\delta E_c > 1.5$, so that the minimum in Eq. (12) is determined by the first term. (In order to satisfy this additional condition the middle island should be sufficiently smaller than the edge islands.)

The above single-cell analysis is only an approximation, because in the real structure all the cells interact with each other and also the presence of neighboring cells somewhat changes the cell electrostatics. This is why we have carried out extensive numerical simulations of reasonably long shift registers (18 three-island cells). For a given geometry of the circuit we first calculated numerically the inverse capacitance matrix $C_{ij}^{-1}$ and the vectors $\vec{D}_i$ (see Appendix A); then these numbers were fed to a Monte-Carlo program which simulated single-electron tunneling events in the circuit using the "orthodox" theory.[1] The logical input was a relatively long (typically, 16-bit) quasi-random bit sequence, repeated periodically many times.

The simulations have shown that for the geometry presented in Fig. 4, elliptic polarization of the clock field (rather than the simple circular polarization implied above) is essential to provide broad margins. More exactly, the out-of-plane component $A_z$ should be larger than the in-plane component $A_y$, because of the field screening in $z$ direction due to the finite size of the conducting islands. For example, for the circuit with $r/R = 0.3$, $d/R = 1.5$, $b/R = 0.7$, and the intercell period in $y$-direction $l/R = 3$, the best ratio $A_z/A_y$ is close to 1.5. If this is done, sufficiently wide margins for the amplitudes of the bias field are really achievable. For $A_z/A_y = 1.5$, the 18-cell shift register with the parameters specified above operates correctly (at zero temperature and sufficiently low clock frequency) within the range $3.25 < A_y/(e/4\pi\epsilon\epsilon_0 R^2) < 5.1$, corresponding to a margin of $\pm 22\%$. If now $A_y$ is kept constant at $A_y = 4.15\, e/4\pi\epsilon\epsilon_0 R^2$, the allowed range for $A_z/(e/4\pi\epsilon\epsilon_0 R^2)$ is between 4.6 and 8.55, corresponding to a margin of $\pm 30\%$. These margins are much broader than those for the first generation of wireless single-electron devices.[27]

The margins for parameters which destroy the geometric symmetry of the parametron cells are much narrower. Numerical simulations show that for a shift register with the parameters quoted above, the maximum allowable shift of the edge islands of a cell in the opposite directions (parallel to the central island shift) is about $\pm 0.010\, R$. This corresponds to the maximal fluctuation of $\pm 0.4$ degrees of the alignment of the line connecting the edge islands of the cell and the $x$-axis. (A shift of only one island leads to the same effect).

Possibly the situation may be improved by using alternative geometries and charge modes.

## VI. SET PARAMETRON LOGIC GATES

The shift register described in the previous Section is actually a line of inverters. To have a complete set for the arbitrary logic functions we need to have other logic gates (e.g., NAND or NOR), and a circuit with a fan-out more than one ("splitter").

All these functions can be naturally implemented using the geometry shown in Fig. 6. If the clock field rotation causes the signal propagation from the bottom to the top we get a fan-out-two circuit, because the dipole moment of cell $F$ (in its ON state) will determine the charge state of both cell $A$ and cell $B$, set during their OFF→ON switching. On the other hand, if the signal propagates from top to bottom, we get the implementation of a binary logic function (either $F = A.\mathrm{NOR}.B$ or $F = A.\mathrm{NAND}.B$, depending on the asymmetry provided by the background charges or dc bias field $\langle E_s \rangle$ imposed on cell $F$).

In order to verify the operation of this system, we have carried out its numerical simulations in the symmetric single-exciton mode, using the same parameters as above ($r/R = 0.3$, $d/R = 1.5$, $b/R = 0.7$, $l/R = 3$) for each of three shift registers, each of them 6 cells long. The $z$-shift between upper registers was $6R$, while the $y$-spacing between cells $A$ ($B$) and $F$ was $2R$, i.e. slightly less than the spacing $l = 3R$ between cells in each register.

The simulations have shown the following margins for the amplitude components $A_y$ and $A_z$ of the clock field (at zero temperature and relatively low speed). For the fan-out-two gate, at $E_z/E_y = 1.5$, we get correct operation at $3.45 < A_y/(e/4\pi\epsilon\epsilon_0 R^2) < 4.2$, corresponding to a margin of ±9%. For the constant $E_y = 4.15\, e/4\pi\epsilon\epsilon_0 R^2$, the $z$-component should be within the range $4.6 < A_z/(e/4\pi\epsilon\epsilon_0 R^2) < 6.3$ (the margins of ±16%). For the NOR gate, with $E_y = 4.1\, e/4\pi\epsilon\epsilon_0 R^2$, $E_z = 6.15\, e/4\pi\epsilon\epsilon_0 R^2$ (this operating point is within the margins for both the shift register and fan-out circuits) correct operation is achieved for the dc bias field $\langle E_s \rangle$ equivalent to the background charge shift in the range $0.034 < q_0/e < 0.053$ ($q_0 = q_{0,left} = -q_{0,right}$). For the NAND gate with similar parameters

the range is $0.035 < -q_0/e < 0.069$. The difference between the results for the ranges (which should coincide because of the layout symmetry) is explained by the finite set of tested input signal sequences which did not have a symmetry between logical zero and unity. Hence, the true range cannot be wider than the common part of two ranges $[0.035, 0.053]$, and thus the real margin is slightly below $\pm 20\%$.

## VII. ENERGY DISSIPATION DURING OFF→ON SWITCHING

Let us calculate the energy dissipation during the switching OFF→ON of one SET Parametron cell in a fixed signal field $E_s$. The switching is illustrated in Fig. 7 which shows the energies of three possible states of the cell as functions of time. For a cell charged by one electron the letters $l$, $r$, and $m$ correspond to the location of the extra electron. For the single-exciton case we can use the same notation, counting one hole or electron as background charge.

Within the framework of the "orthodox" theory the switching is described by the master equation,[1]

$$\begin{aligned} &\frac{d}{dt}\sigma_{l(r)} = \sigma_m \Gamma^+_{l(r)} - \sigma_{l(r)} \Gamma^-_{l(r)} \,, \\ &\frac{d}{dt}\sigma_m = \sigma_l \Gamma^-_l + \sigma_r \Gamma^-_r - \sigma_m (\Gamma^+_l + \Gamma^+_r) \,, \\ &\sigma_m + \sigma_l + \sigma_r = 1 \,, \;\; \sigma_m(-\infty) = 1 \,, \end{aligned} \tag{13}$$

where $\sigma_m$, $\sigma_l$, $\sigma_r$ are the probabilities of finding the system in "$m$", "$l$", and "$r$" states. The tunneling rates $\Gamma^{\pm}_{l(r)}$ are given by Eq. (6), in which we now assume the linear dependence of the energies on time:

$$W^+_r(t) = -W^-_r(t) \equiv W(t) = \alpha t \tag{14}$$

$$W^+_l(t) = -W^-_l(t) = W(t) - \Delta. \tag{15}$$

(This assumption is evidently valid only if the energy difference $\Delta$ due to the signal field in the moment of switching is much less than the maximal energy due to the rotating bias

field.) We also assume that the signal field makes state "$r$" energetically more preferable, $\varepsilon_l - \varepsilon_r = \Delta > 0$.

If the clock speed and temperature are sufficiently low so that the system switches correctly from "$m$" to "$r$" (bit errors will be considered in Section IX), then the energy dissipation can be calculated considering only states "$r$" and "$m$" and neglecting state "$l$". In this case the master equation (13) is simplified with the condition $\sigma_l(t) = 0$,

$$\frac{d}{dt}\sigma_r = (1-\sigma_r)\Gamma^+ - \sigma_r\Gamma^- \tag{16}$$

(here we omit index $r$ in tunneling rates for simplicity), and has an explicit solution

$$\sigma_r(t) = \int_{-\infty}^{t} \Gamma^+(t') \exp\left[-\int_{t'}^{t} \Gamma_\Sigma(t'')dt''\right] dt' , \tag{17}$$

where

$$\Gamma_\Sigma(t) = \Gamma^+ + \Gamma^- = \Gamma^+ \left[1 + \exp(-W(t)/T)\right] . \tag{18}$$

The statistical average of energy loss by the moment $t$ is given by the expression

$$\mathcal{E}(t) = \int_{-\infty}^{t} W(t')\dot{\sigma}_r(t')dt' . \tag{19}$$

Using Eq. (17) we find, finally:

$$\begin{aligned}\mathcal{E}(t) = \int_{-\infty}^{t} W(t')\Gamma_\Sigma(t') \Bigg[ & \frac{1}{1+\exp(-\frac{W(t')}{T})} \\ & - \int_{-\infty}^{t'} \Gamma_\Sigma(t'') \frac{1}{1+\exp(-\frac{W(t'')}{T})} \\ & \times \exp[-\int_{t''}^{t'} \Gamma_\Sigma(t''')dt'''] \, dt'' \Bigg] dt' .\end{aligned} \tag{20}$$

The solid line in Fig. 8 shows the total energy loss $\mathcal{E} = \mathcal{E}(\infty)$ as a function of the dimensionless switching speed

$$\beta \equiv \alpha e^2/GT^2. \tag{21}$$

In the low-speed limit, $\beta \ll 1$, the switching process is almost adiabatic. It consists of numerous tunneling events (back and forth between "$m$" and "$r$" states) occurring within

the energy interval on the order of the thermal energy $T$ around the point $W(t) = 0$. (Figure 7 shows a particular Monte-Carlo realization for $\beta = 0.1$.) It is easy to check that in the purely adiabatic case when $\sigma_r$ is determined by thermodynamics only,

$$\sigma_r(t) = \sigma_r^{ad}(t) \equiv \frac{\Gamma^+}{\Gamma_\Sigma} = \frac{1}{1 + \exp(-W(t)/T)}\,, \tag{22}$$

the total dissipation is zero, because in Eq. (19) the symmetric function of time $\dot{\sigma}_r(t)$ is multiplied by the antisymmetric function $W(t)$.

According to Eq. (16), the correction to the adiabatic limit, $\Delta\sigma_r \equiv \sigma_r - \sigma_r^{ad}$ satisfies the equation $\Delta\sigma_r = -\dot{\sigma}_r/\Gamma_\Sigma$; hence, as the first approximation in $\beta$ we can use

$$\Delta\sigma_r = -\dot{\sigma}_r^{ad}/\Gamma_\Sigma. \tag{23}$$

After the integration by parts of Eq. (19) the total dissipation is given by

$$\mathcal{E} = \int_{-\infty}^{\infty} W(t)\,\frac{d\Delta\sigma_r}{dt}\,dt = -\int_{-\infty}^{\infty} \frac{dW(t)}{dt}\,\Delta\sigma_r\,dt\,. \tag{24}$$

Combining Eqs. (23), (24), (14), (18), and (6), we obtain the low-speed approximation for the total dissipation

$$\mathcal{E} = \kappa\beta T = \kappa\frac{\alpha e^2}{GT}\,, \tag{25}$$

$$\kappa = \int_{-\infty}^{\infty} \frac{e^{-x}(1-e^{-x})}{x(1+e^{-x})^3}\,dx \simeq 0.426\,. \tag{26}$$

In this quasi-reversible regime $\mathcal{E} \ll T$; notice also that in this limit the total dissipation *decreases* when temperature *increases*.

In the opposite limit, $\beta \gg 1$, the speed of energy change is so high that the tunneling occurs only at $W > 0$ and only once – see Fig. 7, without numerous back and forth processes. (Actually, this limit is the only one possible at $T = 0$.) Then the solution of Eq. (16) is

$$\begin{aligned}\sigma_r(t) &= 1 - \exp\left(-\int_0^t \Gamma^+(t)dt\right) \\ &= 1 - \exp\left(-\frac{\alpha G t^2}{2e^2}\right),\ t > 0,\end{aligned} \tag{27}$$

and the average total dissipation

$$\mathcal{E} = (\pi\beta/2)^{1/2}T = (\pi e^2\alpha/2G)^{1/2}. \tag{28}$$

Hence, in the case $\beta \gg 1$ the average energy dissipation is much larger than (and independent of) the thermal energy, indicating the thermodynamic irreversibility of the switching process in this limit. In Fig. 8 the low-speed and high-speed approximations (Eqs. (25) and (28)) are represented by dashed lines, while the solid line shows the result of the exact calculation using Eq. (16), which gives a natural crossover between these two limits.

Equation (6) is valid only for the case of the continuous spectrum of electron energies in the conducting islands. It is easy to consider a different case when the electron energy in the middle island is strongly quantized so that only one level is involved in tunneling, while the energy spectrum of the edge island is still continuous. (This situation is possible when the middle island is much smaller). Then the "orthodox" theory should be somewhat modified,[43–45] however, for our purpose the only important change is that Eq. (6) should be replaced with

$$\begin{aligned} &\Gamma(W) = \frac{\Gamma_0}{1+\exp(-W/T)}, \\ &\Gamma(W) + \Gamma(-W) = \Gamma_0 = \text{const}, \end{aligned} \tag{29}$$

where $\Gamma_0$ is a constant which characterizes the tunnel barrier transparency. Equation (20) yields that the average total energy loss during one switching is given by a simple formula

$$\mathcal{E} = \alpha/\Gamma_0 \tag{30}$$

for arbitrary switching speed (see Fig. 9). It is evident that quasi-reversibility ($\mathcal{E} \ll T$) is possible in this case as well, if the switching speed is low enough: $\alpha \ll T/\Gamma_0$.

In both cases considered above, electron energy relaxation in islands with continuous spectrum (implied by Eqs. (6) and (29)) is the source of dissipation in the system. In the important case when electron energy is quantized in *all* islands this may not be true, so that this limit requires a completely different treatment. Our hope is to complete an analysis of this important case in the near future.

To conclude this section, notice that our model allows not only the total dissipation $\mathcal{E}$ to be calculated, but also the time dynamics of the heat transfer between the system and the environment ("heat bath") during the switching process to be followed. Dashed lines in Figs. 8 and 9 show the results of such calculation using Eqs. (6) and (29), respectively. During the first part of the switching process (when $W(t) \leq 0$) the energy $\mathcal{E}_1 \equiv -\mathcal{E}(0)$ is (on the average) *borrowed* from the heat bath which, hence, is *cooled*. During the second part of the process ($W(t) \geq 0$) the average energy $\mathcal{E}_2 \equiv \mathcal{E} - \mathcal{E}(0) > \mathcal{E}_1$ is *returned* back to the heat bath. Notice that in the adiabatic limit $\mathcal{E}_1 = \mathcal{E}_2 = T \ln 2$ independently of the exact model used for $\Gamma(W)$. This result follows from Eqs. (19) and (22) after the integration by parts:

$$\mathcal{E}_1^{ad} = \mathcal{E}_2^{ad} = \int_{-\infty}^{0} \frac{1}{1+\exp(-W/T)}\, \dot{W}\, dt = T \ln 2. \tag{31}$$

Notice that this is valid for any gradual function $W(t)$, if only $W(0) = 0$.

The generality of this result is due to the direct relation $\mathcal{E}(t) = -T\Delta S_{inf}(t)$ between the energy and the informational ("Shannon") entropy $S_{inf}$ of the degree of freedom used to code information (for a more detailed discussion, see Appendix B). In fact, in the instant when $W = 0$, the system may be in either of two states ($\sigma_m = \sigma_r = 1/2$), hence $\Delta S_{inf} = \ln 2$ has been acquired in comparison with the definite initial state ($\sigma_m = 1$, $\sigma_r = 0$). By the end of the switching the informational entropy is restored to the initial value since the state is definite again ($\sigma_m = 0$, $\sigma_r = 1$). Finite switching speed decreases $\mathcal{E}_1$ and increases $\mathcal{E}_2$ (see the dotted lines in Figs. 8 and 9) leading to a positive total dissipation $\mathcal{E} = \mathcal{E}_2 - \mathcal{E}_1$.

## VIII. REVERSIBLE COMPUTATION

The general thermodynamic arguments lead to the conclusion that erasure of information necessarily requires an energy dissipation of at least $T \ln 2$ per bit (see Refs.[46–48] and Appendix B). During the switching OFF→ON of a cell in any SET-Parametron circuit, the amount of information is not changed, thus allowing arbitrary small energy dissipation in the slow-switching limit. However, for switching ON→OFF the lower bound on dissipation is determined by logical reversibility of a particular circuit.

The SET Parametron shift register is obviously a logically reversible circuit, because during cell switching to OFF the information is preserved by the next cell. It is easy to check (see Fig. 4) that the sign of the energy difference $\Delta = \varepsilon_l - \varepsilon_r$ between two digital states does not change during the ON phase because of the back influence from the next cell. So the cell stays in the lower-energy state and the analysis of the energy dissipation during switching ON→OFF is equivalent to that of the switching OFF→ON (see Fig. 10). A similar small-dissipation case is realized in the SET Parametron fan-out circuit, because during the ON→OFF switching of the last cell of the input line (cell $F$ in Fig. 6) the proper sign of $\Delta$ is maintained by both first cells of the output lines.

The situation is different for the NAND/NOR gate because any gate consisting of two inputs and one output is logically irreversible and, hence, has a lower bound for dissipation.[46–48] For two uncorrelated input streams of bits with equal probabilities of unity and zero, the informational entropy before the logic operation is $S_{inf}^{before} = -\ln(1/4)$ while after the completion of the logic operation and erasure of the input information it becomes $S_{inf}^{after} = -\ln(1/2)$. (Notice that the informational entropy *decreases*. This seems to contradict the apparent partial loss of information at computing. Actually the *uncertainty* is partially lost, not the information, because in the Shannon formalism we should treat the input data as unknown, and the data bit count is decreased by the gate.) The entropy difference determines the lower bound for the average dissipation $\mathcal{E}$ per logic operation $\mathcal{E} \geq T(S_{inf}^{before} - S_{inf}^{after}) = T \ln 2$.

Actually, in the SET Parametron realization shown in Fig. 6 the average energy dissipation is much larger than this lower bound. If two input bits are different, the energy difference $\Delta$ changes its sign during ON state of either cell A or B. In this case the energy dissipation during switching to OFF is comparable to $|\Delta|$ (see Fig. 10) which should be much larger than the thermal energy because the condition $|\Delta| \gg T$ is necessary to ensure small error probability (see next Section).

To realize *reversible* NOR and NAND operations (which would provide small dissipation) using SET Parametron cells, gates with two inputs and three outputs can be used (see Fig.

11). This idea was suggested[37] for the Parametric Quantron logic gates and can be directly applied to the SET Parametron. The input information is copied to the first cells of two additional shift register lines. If their coupling to the last cells of input lines is stronger than input-output coupling, the proper sign of $\Delta$ is always maintained, and the energy dissipation is arbitrarily small in the slow switching limit.

## IX. BIT ERROR RATE

Kinetic equation (13) allows the calculation of the rate of "classical" digital errors during the SET Parametron cell switching (later we will briefly discuss also the "nonclassical" errors due to cotunneling[49]). The error probability $P$ is given by $\sigma_l(\infty)$. Let us first assume $T = 0$ and calculate the "dynamic" error which occurs when the switching speed $\alpha$ is too high, and the system remains in the initial (symmetric) state up to the moment when tunneling to the upper energy level becomes possible (see Fig. 7 and Eqs. (14) – (15)). Since there is no tunneling back and forth at $T = 0$, the error probability can be found simply as the time integral of the rate of erroneous tunneling $\Gamma_l^+$ multiplied by the probability $\sigma_m$ that no tunneling has yet occurred:

$$P_{dyn} = \int_0^\infty \Gamma_l^+(\varepsilon)\, \sigma_m(\varepsilon)\, \frac{d\varepsilon}{\alpha}\,, \tag{32}$$

$$\sigma_m(\varepsilon) = \exp\left(-\int_0^\Delta \Gamma_r^+(\varepsilon')\frac{d\varepsilon'}{\alpha}\right) \times \exp\left(-\int_0^\varepsilon \left(\Gamma_l^+(\varepsilon') + \Gamma_r^+(\varepsilon'+\Delta)\right)\frac{d\varepsilon'}{\alpha}\right). \tag{33}$$

For the "orthodox" model of the tunneling rate given by Eq. (6),

$$P_{dyn} = K\gamma \exp(-\frac{1}{2\gamma})\,, \tag{34}$$

$$K = \frac{1}{2\gamma} - \frac{\sqrt{\pi}}{4\gamma^{3/2}}\exp(\frac{1}{4\gamma})[1 - \mathrm{Erf}(\frac{1}{2\sqrt{\gamma}})] = 1 + \sum_{n=1}^{\infty}\frac{(2n+1)!}{n!}\,(-\gamma)^n, \tag{35}$$

where $\gamma \equiv \alpha e^2/G\Delta^2$. In order to keep $P_{dyn} \ll 1$, $\gamma$ should be much less than 1, then $K \approx 1$. Equation (34) shows that the dynamic error decreases exponentially with the decrease of the switching speed and even faster than exponentially with the increase of $\Delta$ (factor $\Delta^2$ in the exponent).

For sufficiently small $\alpha$ and/or large $\Delta$ the main contribution to the error probability will be due to the thermally activated processes which populate the symmetrical state "$m$" during the passage of energy $\varepsilon_m$ across $\varepsilon_l$. The probability of this "thermal" error is given by the simple formula

$$P_{therm} = \exp(-\Delta/T) \tag{36}$$

and it prevails over $P_{dyn}$ when $T \gg \alpha e^2/G\Delta$. In the case when both errors are of the same order, the result can be found by the numerical solution of Eq. (13). The total error probability can be estimated as the maximum of the two analytical results presented above: $P \simeq \max(P_{dyn},\, P_{therm})$.

If instead of the "orthodox" model we assume that only one discrete energy level of the middle island participates in tunneling, then using Eq. (29) for the tunneling rate we obtain from Eqs. (32) and (33) the following probability of the dynamic error ($T = 0$):

$$P_{dyn} = \frac{1}{2}\exp(-\frac{\Delta}{\alpha}\Gamma_0)\,. \tag{37}$$

The thermal error is still given by Eq. (36), and it prevails over the dynamic error if $T \gg \alpha/\Gamma_0$.

One more possible source of errors is the higher-order quantum process of cotunneling[49] when two or more electrons tunnel simultaneously through different junctions. For illustration, the lowest energy diagram in Fig. 1b shows the situation when the charge state with higher energy is occupied, and the digital information in the cell is preserved by the energy barrier (higher energy of the symmetric state) due to the bias field. According to the orthodox theory, single-electron tunneling in this case is impossible (at sufficiently low temperature). However, the second-order cotunneling, i.e. simultaneous tunneling of two

electrons (through both junction) brings the system into the lower energy state and, hence, is energetically allowed. This process changes the sign of the cell dipole moment and can lead to the digital error.

This type of error can occur, for example, in the 3-phase shift register during the phase when the bit is stored by only one cell, and the long-range interaction with cells carrying other bits (nearest cells are OFF) provides uncontrolled sign of the energy difference between "$l$" and "$r$" states. The erroneous bit will then propagate along the shift register.

Though a detailed analysis of cotunneling was not a goal of this work, we should notice that several means are readily available to reduce the resulting error probability. First, because the rate of $m$-electron cotunneling scales as $(GR_Q)^m$ (where $R_Q \approx 6.5$ $k\Omega$ is the quantum unit of resistance) while the single-electron rate is proportional to the first power of $G$, the decrease of $G$ decreases the relative importance of the cotunneling processes. Another, more powerful method is to increase the smallest order $m$ of possible cotunneling processes. This can be done, for example, by increasing the number of islands per cell. If the cell consists of 5 islands and the ON state corresponds to an electron on one of the outer islands, then at least the 4-th order cotunneling ($m = 4$) is necessary to switch between logical zero and unity; a further increase of the number of islands per cell makes the cotunneling rate negligible even for relatively large tunnel conductance. Finally, it is possible to increase the minimal cotunneling order while still using three-island cells, by increasing the number of cells which store the same bit. This can be done, for example, by the increase of the number of phases in the operation of the shift register. In the realization shown in Fig. 4 this may easily be achieved by a decrease of the angle $\theta$ between the planes of neighboring cells. If the bit is stored by $k$ neighboring cells then the error can occur only if all these $k$ cells will simultaneously change their polarizations and if the final state has a lower energy (any "partial" switching would cost at least one cell-cell interaction energy and, hence, is thermodynamically forbidden at least for not too large $k$). So, the lowest order of erroneous cotunneling is $2k$, and the linear increase in "hardware" allows the exponential reduction of the error probability. This method is applicable to any logic gates which use shift registers

as their input and output lines.

## X. DISCUSSION

In this paper we have presented a functionally complete logic family based on the SET Parametron cells, including inverter, fan-out-two, NAND and NOR gates. All the circuits may operate correctly in a common range for the bias field amplitude. The important advantages of the SET Parametron logic are wireless operation and extremely low power dissipation possible in the quasi-reversible mode of operation, with the energy loss much less then $k_B T \ln 2$ per bit.

While the realization of room temperature operation of the SET parametron logic requires sub-one-nanometer fabrication technology which is hardly available at the present time, the operation of simple SET Parametron circuits (with clock wires) can be readily demonstrated experimentally at lower temperatures. An obvious choice is the aluminum shadow-mask evaporation technology, widely accepted for singe-electron device fabrication (see, e.g., the collection[2]) . Figure 12 shows the sketch of a possible layout of the two-cell SET Parametron shift register-inverter. (For the sake of simplicity, the artifact islands typical for this technology are not shown). Each cell consists of three islands. The capacitive gates are used for the application of rf "clock" fields which cause the switching processes, and simultaneously for the application of dc fields to compensate random background charges. Input gates A and B (for the initial demonstration, one gate is sufficient) determine the polarization of the first cell during its OFF→ON switching. This polarization in turn determines the polarization of the next cell during its OFF→ON switching. The final polarization of the latter cell is sensed by a capacitively coupled single-electron transistor. (If a multilayer fabrication is available, this layout may be further improved to provide wider parameter margins: an overlap (without tunneling) of the edge islands of two cells would increase their capacitive coupling, while a similar overlap of the bias gates with the islands would allow smaller cross-talk.) The operation temperature of such a SET-Parametron circuit with

100-nm-scale tunnel junctions will be in sub-1-K range.

Coming back to the wireless realization, let us estimate the parameters of a possible implementation of the device using the conducting (e.g., metallic) clusters as islands. For a cluster diameter $2R$ about 5 nm (which is at the limit of present-day direct e-beam writing techniques) the charging energy $E_c \sim e^2/8\pi\epsilon\epsilon_0 R$ is about $0.15eV$ (where $\epsilon \sim 2$ is taken as a typical dielectric constant for the organic materials which are the natural candidates for the cluster environment). For the layouts considered in this paper the typical energy difference $\Delta$ between "$l$" and "$r$" states is about $0.2E_c$ leading to $\Delta \sim 0.03$ eV. Requiring the probability of the thermal error to be less than $10^{-10}$ per switching, Eq. (36) yields the maximal operation temperature of about 15 K. Assuming the same value for the dynamic error (then $\gamma \simeq 0.025$ – see Eq. (34)) and taking into account the particular geometry (Fig. 4), we obtain the maximum clock frequency $\nu_{max} \sim 5\times10^{-4}G\Delta/e^2$ that corresponds to about $10^9$ Hz for our parameters and $G \sim(10^5$ Ohm$)^{-1}$ (higher $G$ would make the cotunneling a problem). In this case the power dissipation (see Eq. (28)) is about $4(\pi\gamma/2)^{1/2}\nu\Delta \sim \nu\Delta \sim 5 \times 10^{-12}$ W per cell. This extremely low dissipation would make possible an integration level up to $10^{11}$ cells per cm$^2$ (i.e. $10^3$ nm$^2$ per cell), limited by the cell size, since at 15 K the heat flux about 1W/cm$^2$ can be easily managed without the circuit overheating. To achieve the quasi-reversible mode of operation the frequency should be even lower: $\nu \ll 5 \times 10^7$ Hz for our set of parameters at $T = 15$ K. Accepting, for example, $\nu = 10^6$ Hz we get a power dissipation of only about $5 \times 10^{-18}$ W per cell. This figure indicates that as far as power dissipation is concerned, three-dimensional integration of SET Parametron circuits is quite feasible. Despite the not very spectacular clock frequency in this regime, the total computing performance of a 3D system can be very large.

The largest problem with SET Parametron circuits (besides their fabrication) is that their operation requires well-defined background charges. The allowed fluctuations are only on the order of $0.01e$ (this number corresponds to the maximum tolerated angle of the cell tilt – see Section V). This is a common problem for any single-electron logic (see for example Refs.[4,21,22]). However, if/when a molecular technology becomes available for the

implementation of single-electron and other nanoscale devices, SET Parametron cells may be reproducible on the molecular level, and well defined background charges seem to be achievable in principle.

From the estimates above we see that in order to increase the operation temperature of SET Parametron circuits up to 300 K or even up to 77 K, sub–nanometer-scale islands are necessary. In this case the energy level discreteness[43–45] may result in radically new features of the SET Parametron operation, and should be taken into account at its quantitative analysis. Such analysis is outside the scope of the present paper. We would just like to notice in passing that the operation of SET Parametron circuits in that mode would be rather close to the recently proposed new version[32] of the so-called "Quantum Cellular Automata".[31] This new version, put forward under the keywords of "adiabatic switching" and "pipelining", may remove the principal difficulties[27] of the initial suggestion. We are not, however, aware of any detailed analysis of this new family of logic devices.

## ACKNOWLEDGMENTS

We would like to thank D. V. Averin and T. Usuki for useful discussions. The work was partially supported by AFOSR Grant No. F49620-95-1-0044, Russian RFBR Grant No. 97-02-16332, and Russian Program on Nanoelectronics Grant No. 039-03-232/78/4-3.

## APPENDIX A:

In this Appendix we discuss the method of multiple electrostatic images used to calculate the inverse capacitance matrix $C^{-1}$ and vectors $D$ (island dipole moments) which describe the influence of the external electric field for the arbitrary system of conducting spheres. This method was also used for numerical calculations in another work.[27]

It is well known that the electrostatic field of a point-like charge $q$ located at a distance $d$ from the center of an uncharged sphere having the radius $r$, may be treated as the net field of the charge $q$ and a pair of fictitious charges located inside the sphere, in free space.

The image charge $-qr/d$ is located at the distance $r^2/d$ from the sphere center (in the same direction as the charge $q$), and the compensating charge $qr/d$ is located at the sphere center. The total field of these three charges makes the sphere surface equipotential with $\phi = q/4\pi\epsilon_0 d$.

Let us use this method to calculate the inverse capacitance matrix of two spheres with radii $r$ and $R$, with distance $d$ between the centers. For that, we need to calculate the electrostatic potential when a charge $q$ is placed on the sphere $R$. First, let us create the pair $\mp qr/d$ inside the sphere $r$ (as if we had a point-like charge $q$). Three charges provide the equipotentiality of the sphere $r$, but not sphere $R$. So, we need to create two more charge pairs inside sphere $R$ to restore its equipotentiality. One pair (image of the image charge) will have charges $\pm qd/r \times R/(d - r^2/d)$ and the other pair (image of the compensating charge) will have charges $\mp qd/r \times R/d$ (notice that one charge from each pair is positioned at the center of sphere $R$). Now the equipotentiality of the sphere $r$ is lost again and we need to create four new pairs inside it (actually, three pairs because the position of two charges at the center of $R$ coincides). We can continue this procedure until the charges of new pairs become sufficiently small, and the sphere potentials calculated at each iteration converge with the required accuracy.

The same method is trivially generalized to an arbitrary number of spheres: we need to make images of all charges in all spheres. The method is very simple mathematically but cannot be applied in a straightforward way if the number $N$ of spheres is large, because the number of required image pairs scales as $N^n$ where $n$ is the number of iterations. If $N \sim 100$ and $n \sim 20$ (that is a typical number of necessary iterations if the spheres are close to each other, and we require a good accuracy), then the computer memory will obviously be insufficient.

To solve this problem we use three ways (levels) of storage of information about the pairs, depending on their magnitude (the pair magnitude can be characterized by two numbers: the distance between the charges and the dipole moment of the pair). For "large" pairs we store the whole information (position and the charge magnitude). When the image of a

sufficiently "small" pair is calculated, we store only the location and the magnitude (dipole moment) of the dipole consisting of two image charges, and the total charge at the sphere center. The lowest level of the information representation is to consider the dipole being located at the center of the sphere, so we can sum up all the dipole moments.

This modification of the algorithm allows us to calculate the capacitance matrix for a few hundred spheres with a typical distance between the spheres as small as one tenth of the sphere radius using a modest personal computer. (More closely located spheres require a larger number of image charges.)

The calculation of the $D$ vectors is analogous to the calculation of the inverse capacitance matrix. For example, to determine the influence of $E_x$ field we calculate first the dipole moments (which will have only $x$-component) produced by the field in the independent-sphere approximation. Then we use the iteration procedure described above to restore the equipotentiality of all spheres. At this stage image dipoles (with all spatial components) as well as image charge pairs appear. The island potentials for the unit external field $E_x$ are the components of the $D$ vector corresponding to $x$-axis (we need three $D$ vectors for three dimensions).

## APPENDIX B:

In this Appendix we discuss the heat transfer during the adiabatic transition (switching) between an arbitrary number of charge states. This analysis can be used for the fan-out circuits and for SET Parametron cells consisting of more than three islands. The formalism was developed long ago[46–48] and constitutes the basis of the reversible computation analysis giving the lower bound for the energy dissipation for irreversible logical gates.

The infinitesimal heat transfer to the thermal bath can be written as

$$dQ = \sum_{i,j} (\varepsilon_i - \varepsilon_j)\, \sigma_i\, \Gamma_{i\to j}\, dt = -\sum_i \varepsilon_i\, d\sigma_i\,, \tag{B1}$$

where $\varepsilon_i$ is the (free) energy of the state $i$, $\sigma_i$ is its probability, $d\sigma_i$ is the probability change during the interval $dt$, and $\Gamma_{i\to j}$ is the rate of transition from state $i$ to state $j$ (i.e.

the corresponding tunneling rate). In the thermodynamically reversible adiabatic limit the probabilities satisfy the equilibrium distribution

$$\sigma_i = \sigma_{i,ad} = Z^{-1} \exp(-\varepsilon_i/T),\ Z = \sum_i \exp(-\varepsilon_i/T). \tag{B2}$$

Using the definition of Shannon's informational entropy[46]

$$S_{inf} = -\sum_i \sigma_i \ln \sigma_i \,, \tag{B3}$$

and using the evident equation $\sum_i d\sigma_i = 0$ we get

$$dS_{inf} = -\sum_i d\sigma_i (1 + \ln \sigma_i) = T^{-1} \sum_i \varepsilon_i \, d\sigma_i. \tag{B4}$$

We see that in the adiabatic case

$$dQ = -T \, dS_{inf}. \tag{B5}$$

It is not difficult to prove that in the general (nonadiabatic) case $\delta Q \geq -T \, dS_{inf}$. Let us introduce the difference

$$X \equiv \frac{\delta Q}{T} + dS_{inf} = -\sum_i d\sigma_i \ln \frac{\sigma_i}{\sigma_{i,ad}} \,. \tag{B6}$$

Using the general master equation

$$\frac{d\sigma_i}{dt} = \sum_j \sigma_j \Gamma_{j\to i} - \sigma_i \sum_j \Gamma_{i\to j} \tag{B7}$$

to substitute $d\sigma_i$ in Eq. (B6), making the resulting expression symmetric over indices $i$ and $j$, and using the general thermodynamic relation for the tunneling rates $\Gamma_{i\to j}/\Gamma_{j\to i} = \exp((\varepsilon_i - \varepsilon_j)/T)$ (c.f. Eqs. (18) and (29)) we obtain

$$\begin{aligned} X/dt = -\sum_{i,j} \Gamma_{i\to j} \Bigg[ & -\sigma_i \ln \frac{\sigma_i}{\sigma_{i,ad}} \\ & +\sigma_j \ln \frac{\sigma_i}{\sigma_{i,ad}} \exp(\frac{\varepsilon_j - \varepsilon_i}{T}) \\ & -\sigma_j \ln \frac{\sigma_j}{\sigma_{j,ad}} \exp(\frac{\varepsilon_j - \varepsilon_i}{T}) + \sigma_i \ln \frac{\sigma_j}{\sigma_{j,ad}} \Bigg] . \end{aligned} \tag{B8}$$

After the simple transformations and using Eq. (B2) we finally get the expression

$$X/dt = -\sum_{i,j} \Gamma_{i\to j} \ln\left(\frac{\sigma_i}{\sigma_j \exp(\frac{\varepsilon_j-\varepsilon_i}{T})}\right) \times \left(\sigma_j \exp(\frac{\varepsilon_j-\varepsilon_i}{T}) - \sigma_i\right) \tag{B9}$$

which is obviously positive or zero. This proves the general inequality

$$\delta Q \geq -T\, dS_{inf}\,. \tag{B10}$$

Notice that if we introduce also the "usual" entropy $\tilde{S}$ so that $\delta Q = T\, dS$, then the total entropy $S_t = S_{inf} + \tilde{S}$ is constant in the adiabatic case. In the general case, the total entropy is a non-decreasing function of time, $dS_t/dt \geq 0$, while the decrease of $\tilde{S}$ is not forbidden.

# REFERENCES


[1] D. V. Averin and K. K. Likharev, in *Mesoscopic Phenomena in Solids*, edited by B. L. Altshuler *et al.*, (Elsevier, Amsterdam, 1991), p. 173.

[2] *Single Charge Tunneling*, edited by H. Grabert and M. H. Devoret (Plenum, New York, 1992).

[3] D. V. Averin and K. K. Likharev, in Ref.[2], p. 311.

[4] A. N. Korotkov, in *Molecular Electronics*, edited by J. Jortner and M. Ratner (Blackwell, Oxford, 1997), p. 157.

[5] D. V. Averin and K. K. Likharev, J. Low Temp. Phys. **62**, 345 (1986).

[6] T. A. Fulton and G. C. Dolan, Phys. Rev. Lett. **59**, 109 (1987).

[7] K. K. Likharev, IEEE Trans. Magn. **23**, 1142 (1987).

[8] H. Pothier, P. LaFarge, R. F. Orfila, C. Urbina, D. Esteve, and M. H. Devoret, Physica B **169**, 573 (1991).

[9] M. W. Keller, J. M. Martinis, N. M. Zimmerman, and A. H. Steinbach, Appl. Phys. Lett. **69**, 1804 (1996).

[10] K. K. Likharev, N. S. Bakhvalov, G. S. Kazacha, and S. I. Serdyukova, IEEE Trans. Magn. **25**, 1436 (1989).

[11] K. P. Hirvi, J. P. Kauppinen, A. N. Korotkov, M. A. Paalanen, and J. P. Pekola, Appl. Phys. Lett. **67**, 2096 (1995).

[12] P. LaFarge, P. Joyez, H. Pothier, A. Cleland, T. Holst, D. Esteve, C. Urbina, and M. H. Devoret, C. R. Acad. Sci. Paris, Ser. II, **314**, 883 (1992).

[13] P. D. Dresselhaus, L. Ji, S. Han, J. E. Lukens, and K. K. Likharev, Phys. Rev. Lett. **72**, 3226 (1994).

[14] K. Yano, T. Ishii, T. Hashimoto, T. Kobayashi, F. Murai, and K. Seki, IEEE Trans. Electron. Dev. **41**, 1628 (1994).

[15] K. Nakazato, R. J. Blaikie, and H. Ahmed, J. Appl. Phys. **75**, 5123 (1994).

[16] L. Guo, E. Leobandung, and S. Chou, Appl. Phys. Lett. **70**, 850 (1997).

[17] A. Nakajima, T. Futatsugi, and N. Yokoyama, Appl. Phys. Lett. **70**, 1742 (1997).

[18] C. D. Chen, Y. Nakamura, and J. S. Tsai, Appl. Phys. Lett. **71**, 2038 (1997).

[19] K. K. Likharev and A. N. Korotkov, in: *Abstracts of IWCE'95* (Tempe AZ, 1995), p. 42; in: *Proceedings of ISDRS'95* (Charlottesville VA, 1995), p. 355; VLSI Design (Amsterdam) **3**, 201 (1997), and to be published.

[20] J. R. Tucker, J. Appl. Phys. **72**, 43339 (1992).

[21] A. N. Korotkov, R. H. Chen, and K. K. Likharev, J. Appl. Phys. **78**, 2520 (1995).

[22] R. H. Chen, A. N. Korotkov, and K. K. Likharev, Appl. Phys. Lett. **68**, 1954 (1996).

[23] K. K. Likharev and V. K. Semenov, in *Extended Abstracts of International Superconductive Electronics Conference*, Tokyo, 1987, p. 182.

[24] K. K. Likharev, S. F. Polonsky, and S. V. Vyshenskii, "Single-electron logic/memory family", unpublished (1990); see Ref.[3].

[25] Yu. V. Nazarov and S. V. Vyshenskii, in *Single-Electron Tunneling and Mesoscopic Devices*, edited by H. Koch and H. Lubbig (Springer, Berlin, 1992), p. 61.

[26] K. Nakazato and J. D. White, IEDM **1992**, 487 (1992).

[27] A. N. Korotkov, Appl. Phys. Lett., **67**, 2412 (1995).

[28] K. K. Likharev and A. N. Korotkov, in *Abstracts of IWCE'95* (Tempe AZ, 1995), p. 5.

[29] K. K. Likharev and A. N. Korotkov, Science **273**, 763 (1996).

[30] M. G. Ancona, J. Appl. Phys. **79**, 526 (1996).

[31] C. S. Lent, P. D. Tougaw, W. Porod, and G. H. Bernstein, Nanotechnology **4**, 49 (1993).

[32] C. S. Lent and P. D. Tougaw, Proc. IEEE **85**, 541 (1997).

[33] R. A. Kiehl and T. Oshima, Appl. Phys. Lett. **67**, 2494 (1995).

[34] T. Oshima and R. A. Kiehl, J. Appl. Phys. **80**, 912 (1996).

[35] For the sake of simplicity and following the tradition of single-electronics, we will assume that the charge of the uncompensated charge is positive, still referring to it as an electron. This will not affect any finite result.

[36] K. K. Likharev, IEEE Trans. Magn. **15**, 240 (1977).

[37] K. K. Likharev, Int. J. Theor. Phys. **21**, 311 (1982).

[38] K. F. Loe and E. Goto, IEEE Trans. Magn. **21**, 884 (1985); M. Hosoya *et al.*, IEEE Trans. Appl. Supercon. **1**, 77 (1991).

[39] See, e.g., H. Takahashi, J. Inst. Electron. Commun. Eng. of Japan **64**, 1249 (1981).

[40] In principle, an electron can also be in different states (of higher energy) inside each island, but these states are not explicitly participating in the theory of single-electron tunneling, at least in its simplest "orthodox" version.[1]

[41] Using approximation (5) one could expect that for sufficiently large ratio $r/R$ it should be possible to satisfy inequality $2/s - 1/r - 1/2d > 0$ which would lead to $\Delta E_c < \delta E_c$ (simultaneously $\Delta E_s > \delta E_s$). This would "rotate" the phase diagram by 90 degrees, reversing the roles of $E_s$ and $E_c$. However, this conclusion is an artifact of approximation (5) which is too inaccurate when $s-R-r \lesssim \max(R,r)$. Actually the axis reversal described above is impossible since the required relation $2C_{12}^{-1} - C_{22}^{-1} - C_{13}^{-1} > 0$ contradicts the general electrostatic property $C_{13}^{-1} > C_{12}^{-1}C_{23}^{-1}/C_{22}^{-1}$. The latter inequality can be derived calculating the potential of the third island due to the positive charge on the first island

with the grounded second island and requiring the result to be positive.

[42] Notice that because of the double switching per period, the speed of the data propagation is 6 cells per clock cycle, i.e. twice as large as the number of cells per bit (3). There is one more difference between the implementation of the shift register (Fig. 4) and the general scheme shown in Fig. 3: the repulsion of similar electric charges leads to the inversion of the sign of the dipole moment at each register step. Hence the correspondence between the digital bit and the electric moment alternates each next cell.

[43] D. V. Averin and A. N. Korotkov, Sov. Phys. JETP, **70**, 937 (1990).

[44] D. V. Averin, A. N. Korotkov, and K. K. Likharev, Phys. Rev. B **44**, 6199 (1991).

[45] C. W. J. Beenakker, Phys. Rev. B **44**, 1646 (1991).

[46] See, e.g., the collection by H. S. Leff and A. F. Rex, *Maxwell's Demon: Entropy, Information, Computing* (Princeton Univ. Press, Princeton, NJ, 1990).

[47] R. Landauer, IBM J. Res. Devel. **5**, 183 (1961); R. W. Keyes and R. Landauer, *ibid*, **14**, 152 (1970).

[48] C. Bennett, IBM J. Res. Devel. **17**, 525 (1973).

[49] D. V. Averin and A. A. Odintsov, Phys. Lett. A **140**, 251 (1989).

## FIGURES

FIG. 1. SET Parametron: (a) the basic cell and (b) its energy diagrams for three values of the bias field $E_c$ (for discussion, see the text).

FIG. 2. Phase diagrams of stable charge states of a SET Parametron cell with $q_{i0} = 0$, $R/r = 1$, $d/r = 3$, $b/r = 1$, where $2d$ is the distance between outer island centers while $b$ is the $y$-axis shift of the middle island center – see Fig. 1a. (a) The cell is charged with one extra electron; (b) electrostatically neutral cell. $\Delta E_c$ and $\Delta E_s$ are the diagram periods for the clock and signal electric fields, respectively. Bistable regions are shaded. Thick line in (a) illustrates the switching from OFF to ON states, while rectangles in (b) illustrate two possible operation modes of the cell.

FIG. 3. The general idea of the three-phase shift register using parametron-type cells. Each line shows the logical state of the shift register at a particular phase of the clock cycle, dashes indicating the monostable OFF state and **I** representing bistable ON states.

FIG. 4. The top (left) and side (right) views of a shift register based on the single-exciton parametron cells operating in the symmetric mode. The clock field vector $E(t)$ rotates in plane $y - z$. Digital bits are coded by the direction of the cell polarization and are propagated from the top of the figure to the bottom, over 6 cells during one clock period.

FIG. 5. Time diagram illustrating the operation of the shift register shown in Fig. 4. Three sine curves show the in-plane component of the clock field for three neighboring cells. Dots correspond to the points where the middle curve enters or exits the bistable ON regions (shaded), so that the middle cell changes its charge state.

FIG. 6. Circuit which can be used for the fan-out-two splitting of a signal (if the propagation direction is from the bottom to the top), or as a logical gate NAND or NOR (for opposite signal propagation direction). The asymmetry required for NAND and NOR gates can be created by the adjustment of the background charges on the edge islands of cell $F$, or by application of local electrostatic field $\langle E_s \rangle$.

FIG. 7. Energy diagram of the OFF→ON switching. The system, initially in state "m", is switched to state "r" (switching to "l" would give a digital error). Numerous tunneling events (back and forth) occur in the slow switching case $\beta \ll 1$ (a particular result of Monte-Carlo simulation for $\beta = 0.1$ is shown), while for $\beta \gg 1$ there is only one tunneling event.

FIG. 8. Components of the energy exchange between the parametron and the heat bath as functions of the process speed $\alpha = dW/dt$. Dotted lines: average energy flow $\mathcal{E}_1$ from the heat bath to the parametron during the first part of the process (when $W \leq 0$), and the average flow $\mathcal{E}_2$ from the device back into the heat bath during its second part (when $W \geq 0$). Solid line: the net energy dissipation $\mathcal{E} = \mathcal{E}_2 - \mathcal{E}_1$. Dashed lines show the low-speed (Eq. (25)) and high-speed (Eq. (28)) asymptotes.

FIG. 9. The same as in Fig. 8, but for the case of the discrete energy spectrum of the middle island.

FIG. 10. Energy diagram of the ON→OFF switching. If the system initially occupies the state with lower energy, arbitrary small energy dissipation is possible at slow switching (simulation for $\beta = 0.1$ is shown). On the contrary, if the switching starts from the upper state, the energy loss is finite and of the order of $|\Delta|$. (For this case, Monte Carlo simulation has given two almost simultaneous tunneling events shown by arrows).

FIG. 11. Schematics of logically reversible NAND/NOR gate with two input shift-register lines and three output lines. The input information is preserved in two additional output lines.

FIG. 12. Sketch of a possible layout of the two-cell SET-Parametron shift register suitable for the standard double-angle shadow evaporation technique (the artifact islands are not shown).

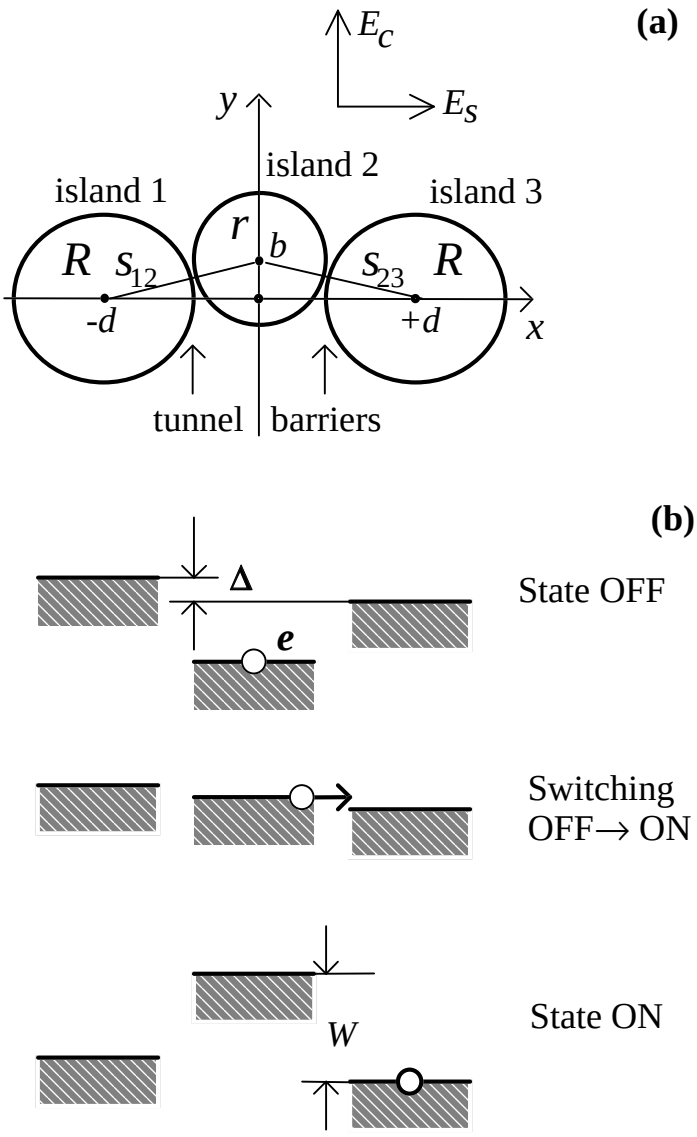
(a)
$E_C$
$E_S$
y
island 1
island 2
island 3
r
b
R
$s_{12}$
$s_{23}$
R
-d
+d
x
tunnel
barriers
(b)
Δ
e
State OFF
Switching
OFF→ ON
W
State ON

Fig. 1

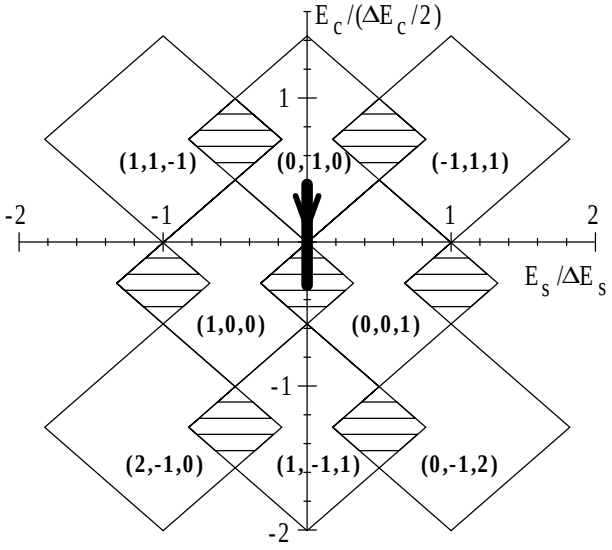
E_c/(ΔE_c/2)
1
(1,1,-1)
(0,1,0)
(-1,1,1)
-2
-1
1
2
E_s/ΔE_s
(1,0,0)
(0,0,1)
-1
(2,-1,0)
(1,-1,1)
(0,-1,2)
-2

Fig. 2a

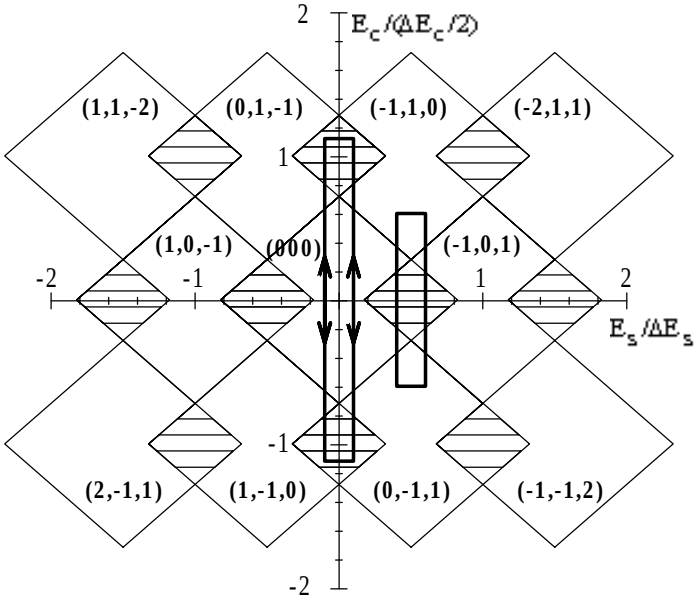
2
E_c/(ΔE_c/2)
(1,1,-2)
(0,1,-1)
(-1,1,0)
(-2,1,1)
1
(1,0,-1)
(000)
(-1,0,1)
-2
-1
1
2
E_s/ΔE_s
-1
(2,-1,1)
(1,-1,0)
(0,-1,1)
(-1,-1,2)
-2

Fig. 2b

| | | | | | | | | | | | | | | |
|---|---|---|---|---|---|---|---|---|---|---|---|---|---|---|
| . . . | $I_4$ | - | - | $I_3$ | - | - | $I_2$ | - | - | $I_1$ | - | - | . . . | time ↓ |
| . . . | $I_4$ | $I_4$ | - | $I_3$ | $I_3$ | - | $I_2$ | $I_2$ | - | $I_1$ | $I_1$ | - | . . . | |
| . . . | - | $I_4$ | - | - | $I_3$ | - | - | $I_2$ | - | - | $I_1$ | - | . . . | |
| . . . | - | $I_4$ | $I_4$ | - | $I_3$ | $I_3$ | - | $I_2$ | $I_2$ | - | $I_1$ | $I_1$ | . . . | |
| . . . | - | - | $I_4$ | - | - | $I_3$ | - | - | $I_2$ | - | - | $I_1$ | . . . | |
| . . . | $I_5$ | - | $I_4$ | $I_4$ | - | $I_3$ | $I_3$ | - | $I_2$ | $I_2$ | - | $I_1$ | . . . | |
| . . . | $I_5$ | - | - | $I_4$ | - | - | $I_3$ | - | - | $I_2$ | - | - | . . . | |

information propagation →

Fig. 3

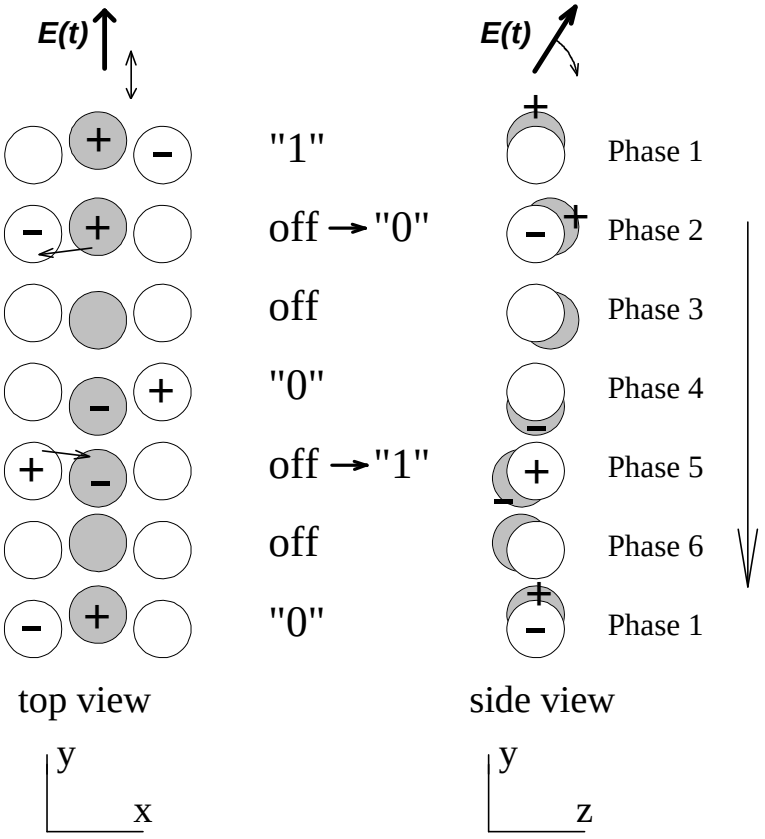


Fig. 4

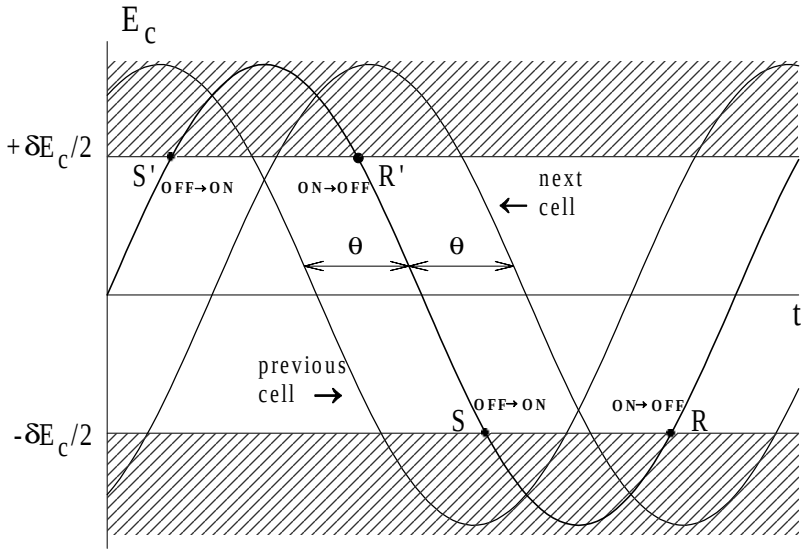
E c
+δE c/2
-δE c/2
S'
OFF→ON
ON→OFF
R'
next
cell
θ
θ
t
previous
cell
S
OFF→ON
ON→OFF
R

Fig. 5

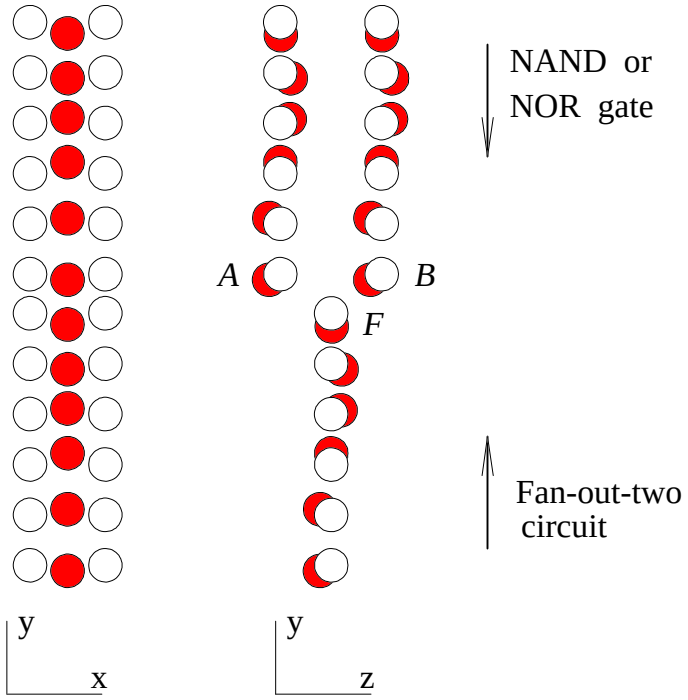
NAND or
NOR gate
A
B
F
Fan-out-two
circuit
y
x
y
z

Fig. 6

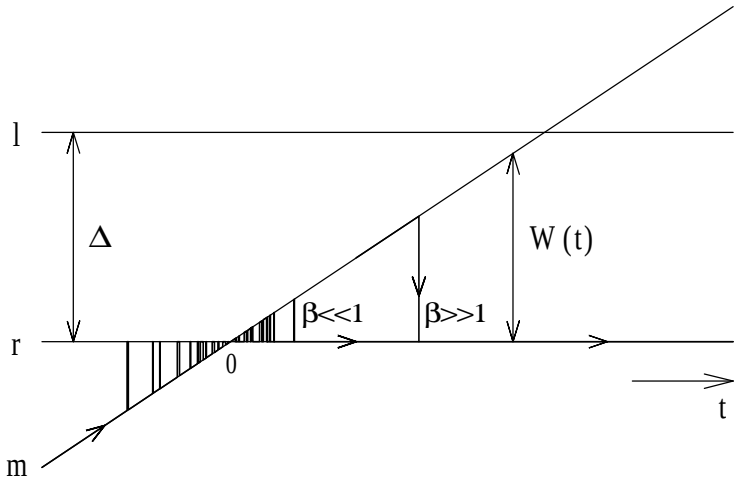


Fig. 7

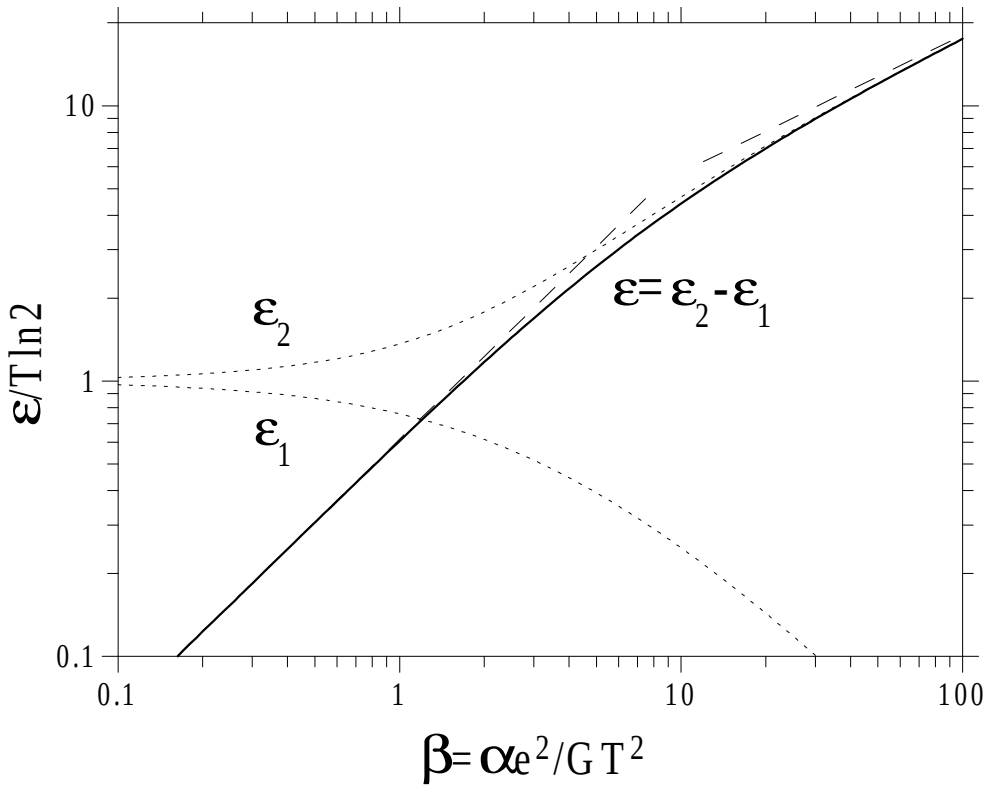


Fig. 8

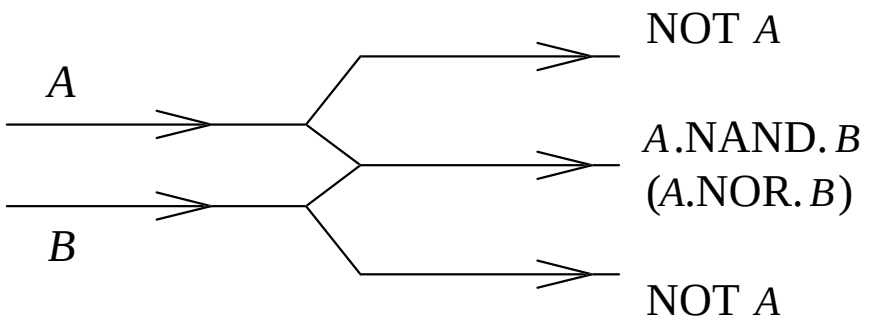
NOT A
A
A.NAND.B
(A.NOR.B)
B
NOT A

Fig. 11

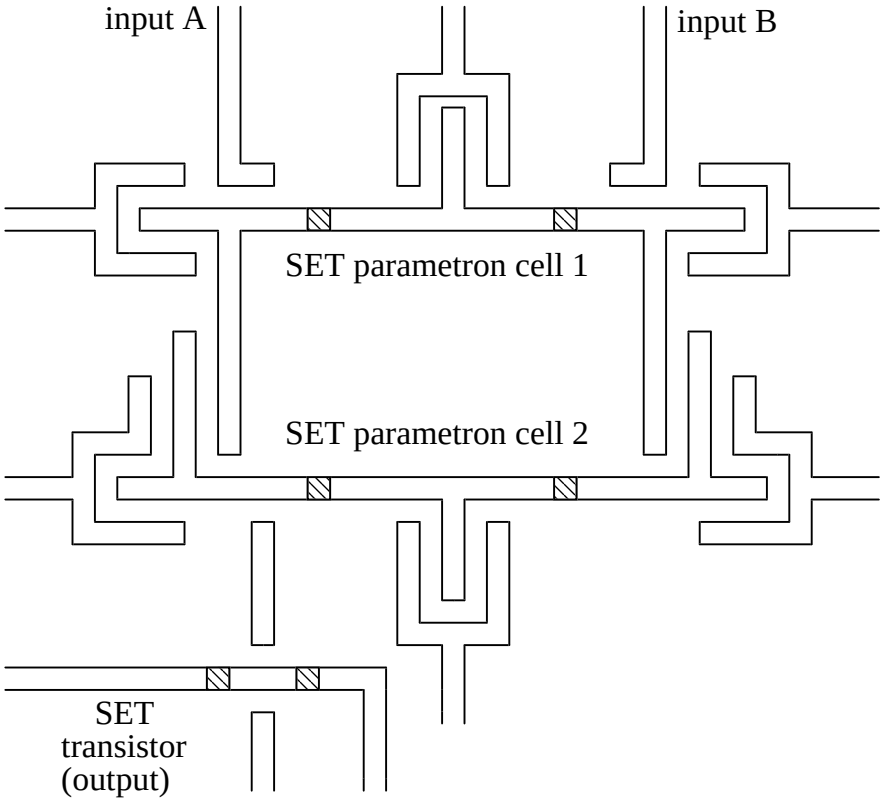
input A
input B
SET parametron cell 1
SET parametron cell 2
SET
transistor
(output)

Fig. 12

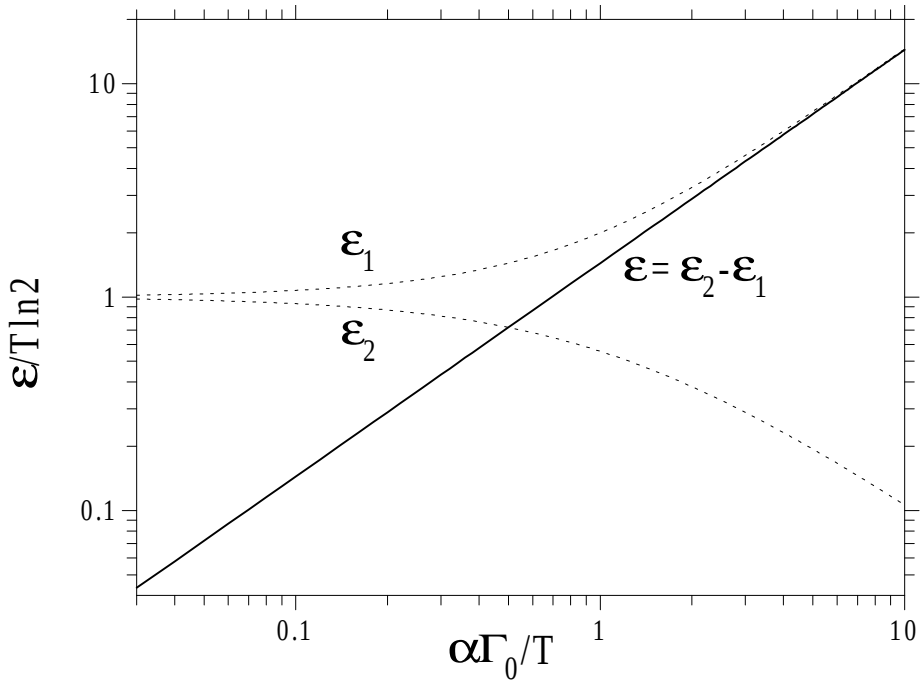
10
1
0.1
ε/Tln2
ε1
ε2
ε= ε2-ε1
0.1
1
10
αΓ0/T

Fig. 9

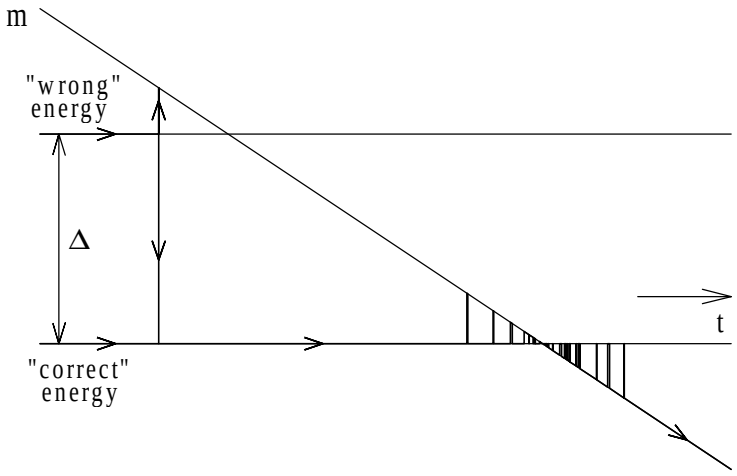
m
"wrong"
energy
Δ
t
"correct"
energy

Fig. 10